ELSEVIER Solar Energy Materials and Solar Cells 53 (1998) 313–327

Solar Energy Materials & Solar Cells

Characterization of multicrystalline silicon: Comparison between conventional casting and electromagnetic casting processes

E. Ehret*

Laboratoire de Physique de la Matière, URA-CNRS 0358, Institut National des Sciences Appliquées de Lyon, 20 Avenue Albert Einstein, 69621 Villeurbanne, France

Received 6 October 1997

Abstract

The multicrystalline silicon produced by different growth processes exhibit quite different chemical, physical and electrical properties. The electrical properties depend in a very complicated manner on the growth history of materials. This study addresses the analysis of the influence of the electromagnetic casting (EMC) growth process on the physical and electrical properties of the materials in order to determine the main limiting factors of this growth method for high-efficiency solar cells. We compare results for the conventional Polix material based on molded ingots supplied by Photowatt. Furthermore, we intend to understand the influence of thermal treatments on the electrical properties of these specific materials. © 1998 Elsevier Science B.V. All rights reserved.

Keywords: Multicrystalline; Silicon; Photovoltaic; Extended defects; Electromagnetic casting

1. Introduction

The probability that manufacturing casting processes of multicrystalline silicon substrates will contribute to the future electricity market is connected with the development of economical production technologies. At present, several different

* Corresponding author. Present address: L.E.S.-L.P.M.O. 4 pl. Tharradin BP 427, 25211 Montbeliard, France. E-mail: eehret@pu-pm.univ-fcomte.fr

PII S0927-0248(98)00022-1

technologies to obtain multicrystalline silicon for the solar cell material are known. They are separated into two groups: the mold techniques, characterized by melting the feedstock within a graphite or quartz crucible and the electromagnetically casting (EMC) technique, recently introduced, in which molten silicon is heated and pinched electromagnetically preventing the metal from coming into contact with the cold crucible wall [1]. The features and the advantages of electromagnetic casting are (i) the simultaneous melting and solidification of metals in one crucible, (ii) the melting and the suspension of metals by electromagnetic force, and (iii) the continuous melting and casting of metals. This new process is expected to reduce the cost of the solar cell production. However, the analysis of the crystal properties could determine if the improvement of economical aspects results in decreased electrical properties of materials and solar cell performance.

As it is well known, the different growth processes exhibit quite different chemical, physical and electrical properties. These differences associated with the particular growth process may affect the grain boundaries and intragranular properties which are dominated by dislocations and eventually by precipitates. It is obvious that the electrical properties depend in a very complicated manner on the growth history of materials. Different studies performed on conventional multicrystalline silicon indicate that the effective diffusion length and the conversion efficiency depend closely on the dislocation density. These studies also show that the role of structural reconstruction of extended defects is secondary with respect to that of the chemical reconstruction originated by the segregation of carbon and oxygen [2,3]. Moreover, the electrical properties of solar cells do not depend only on the material manufacturing process, but they are greatly influenced by the device fabrication. Depending on the temperature and on the time of treatment, impurities segregate or precipitate, eventually introducing local internal stresses. These mechanisms could result in the generation of electrically active defects in solar cells [4].

This study addresses the analysis of the influence of the EMC growth process on the physical and electrical properties of the materials in order to determine the main limiting factors of this growth method for high-efficiency solar cells. We compare results for the conventional Polix material based on molded ingots supplied by Photowatt, and the EMC material produced by SITIX and more recently by EPM-Madylam. Furthermore, we intend to understand the influence of thermal treatments on the electrical properties of these specific materials.

2. Electromagnetic casting process

The schematic furnace assembly, shown in Fig. 1, explains the basic furnace structure. It consists of a silicon material feeding system, an induction cold crucible arrangement, an auxiliary heating equipped to control the temperature of solidified ingot, an ingot supporting and pulling system, and an air-tight furnace chamber.

In the conventional process of melting by induction, the fire-proof crucible is heated by induction and the feedstock is melted by conduction. In the EMC process, the crucible is segmented and each electrically isolated segment is cooled by the

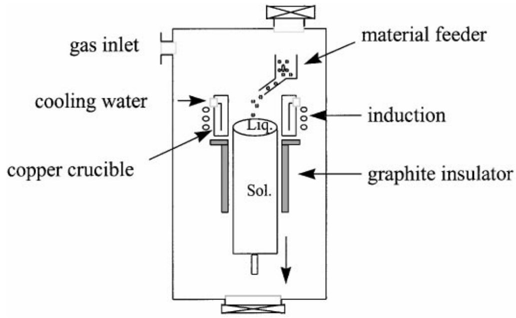

Fig. 1. Schematic explanation of the cold crucible induction casting.

circulation of cooling water throughout the crucible. The crucible is made of copper to obtain good thermal and electrical conductivity. These segments of cooled copper prevent molten metal from coming into contact with the crucible wall by an interactive force of magnetic field and induced electric current.

Induction coils work to melt silicon materials and give rise to magnetic pressure which suspends the molten silicon keeping the melt free of the crucible wall. The induction frequency is one of the most important parameters in using the EMC melting. Indeed, under a magnetic field, induced current spreads out in the superficial zone in the ingot, for which the thickness, δ, varies versus the electrical conductivity, σ, of material and current frequency, f, by the relation

$$\delta = (2/\mu\sigma w) \quad \text{with } w = 2\pi f.$$

The crucible segments permit the induced currents to be near the internal crucible surface. Thus, the currents induced into the charge, heat it by the joule effect and interact with the magnetic field to give Laplace–Lorentz forces mainly distributed in the outer skin of the charge. These forces give rise first to a repulsion effect which repels the liquid from the crucible and secondly to a stirring of molten metal which permits the homogeneity of the silicon melt.

The thermal insulator (graphite fibers) are placed below the crucible and surround the ingot which ensures a good temperature distribution along the axial direction to avoid detrimental thermal stresses. The distance of the cold wall below the inductors, controls a stable shape of solid–liquid interface. When the distance is small, the shell becomes very thin and is easy to break free of the molten silicon. When the distance is large, the solidified shell is thick and the ingot is too chilled to generate thermal stresses.

3. Crystal structure

3.1. Solidification structure

As generally observed in molded crystals, the liquid metal freezes in three stages, distinguished from each other by the size and shape of the grains.

1. The first zone (superficial zone) freezes near the wall of the crucible and consists of relatively fine grains equiaxed in shape and random in orientation. Grain size is less than 1 mm on a section perpendicular to the grown axis and spread out to one-tenth of the ingot radius.
2. The next zone (transition zone) consists of crystals elongated in the direction of heat flow. These crystals are much larger in cross-section than the crystals of the chill zone and have a very strong preferred orientation. This zone spreads out to a 2–4 tenths of the ingot radius and the crystals are fairly disoriented from the growth axis.
3. The final zone (center zone) has a much coarser grain size than the first zone and crystal orientation follows the direction of heat flow quite parallel to the growth axis. The disorientation angle is less than 10°. This is the columnar zone. It spreads out to 5–7 tenths of the ingot radius. The grain size is about 4–5 mm.

A vertical cross-sectional view of the ingot in the dimensions of $120 \times 120\ \mathrm{mm}^2$ horizontal cross-section is shown in Fig. 2. The crystalline growth structure and the distributions of grown grains sizes are clearly observed. The grain sizes grown in the center of the ingot are fairly larger. However, in the circumference of the ingot, the crystalline structure is strongly directional from the surface making the grain size minute.

The grain boundaries spread out parallel to the heat flow direction. The solidification interface is a surface orthogonal to the heating rate lines. It is estimated by

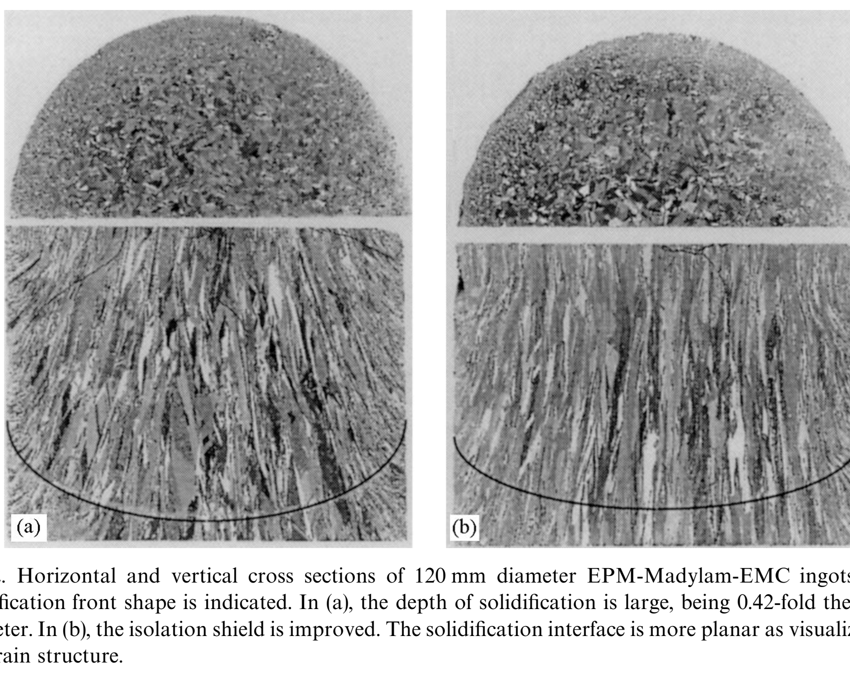

Fig. 2. Horizontal and vertical cross sections of 120 mm diameter EPM-Madylam-EMC ingots. The solidification front shape is indicated. In (a), the depth of solidification is large, being 0.42-fold the ingot diameter. In (b), the isolation shield is improved. The solidification interface is more planar as visualized by the grain structure.

intentionally induced doping striations. The solidification front shape is detected by the change of ingot resistivity. The depth of solidification is large being 0.42-fold the ingot diameter. However, the heat losses under the crucible are lowered by improving the isolation shields. This process results in a solidification interface more planar as visualized by the grain structure in Fig. 2b. Moreover, this modification gives rise to an increase of the central width at the expense of the transition zone width.

At the ingot periphery, the grain growth is started by the cooling effect due to the crucible, just below the horizontal level of the RF coil end. In the three-phase junction formed between the tangents to the melt/gas and the crystal/gas surfaces, the liquid has been cooled to reach a sufficient supercooling which permits the nucleation. Indeed, a dendritic growth due to thermal supercooling occurs. Small grains are formed along the surface from the three-phase junction. It has been shown experimentally that the dendritic growth favors the dendrites growing in the heat flow direction. The mechanism by which the dendrites in the heat flow direction eliminate their unfavorably directed neighbors is explained by Chalmers et al. [5]. This mechanism is effective in our process from the ingot periphery to the transition zone.

The selection occurs and permits the increase of the averaged grain size. The disorientation of grain boundary from the heating rate lines comes to an increase of the grain size as observed in the central zone.

3.2. Etch pits counting and dislocation pattern examination

The dislocation density N_{dis} is systematically determined using the Secco Etch technique on the sample surface. Dislocation density is found larger on the edge of the ingot. In the center, by growing the crystallites parallel, less stress between neighboring crystal is induced. Thus, the dislocation density is lower and seems to be quite uniform. The average value of N_{dis} is varied from 10^4 to about $10^6\ cm^{-2}$. Regions of dislocation agglomerates with $N_{dis} > 2 \times 10^6\ cm^{-2}$ are also observed in EMC EPM-Madylam materials. The values for Polix material are lower and quite uniform with a dislocation density of $8–10 \times 10^4\ cm^{-2}$.

The optical micrographs of etched samples of the EMC EPM-Madylam materials show an important heterogeneity of the crystal structure for different grains. Indeed, areas of large and low dislocation density are contiguous as observed in the Fig. 3a. Fig. 3b shows areas of randomly distributed etch pits. No slip planes are observed. Such an arrangement supposes (i) the existence of a lot of slip planes which originate from severe or multiaxial stresses, or (ii) the tendency of dislocation to move out of their slip planes by climb. The former requires low temperatures and severe stresses and the latter requires high temperatures and lower stresses. Fig. 3c seems to indicate that the movement of dislocations is hampered by the presence of grain boundaries. The dislocations go round these interfaces. This observation suggests that this phenomenon could be provided by the cross slip of dislocations from the easy glide plane which occurs at high temperatures and severe thermal stresses. In Fig. 3d, an arrangement of dislocations in a cell-like shape is observed near the periphery of the ingot. Such arrangement corresponds to a tensile-compressive cycle. Indeed, in the EMC

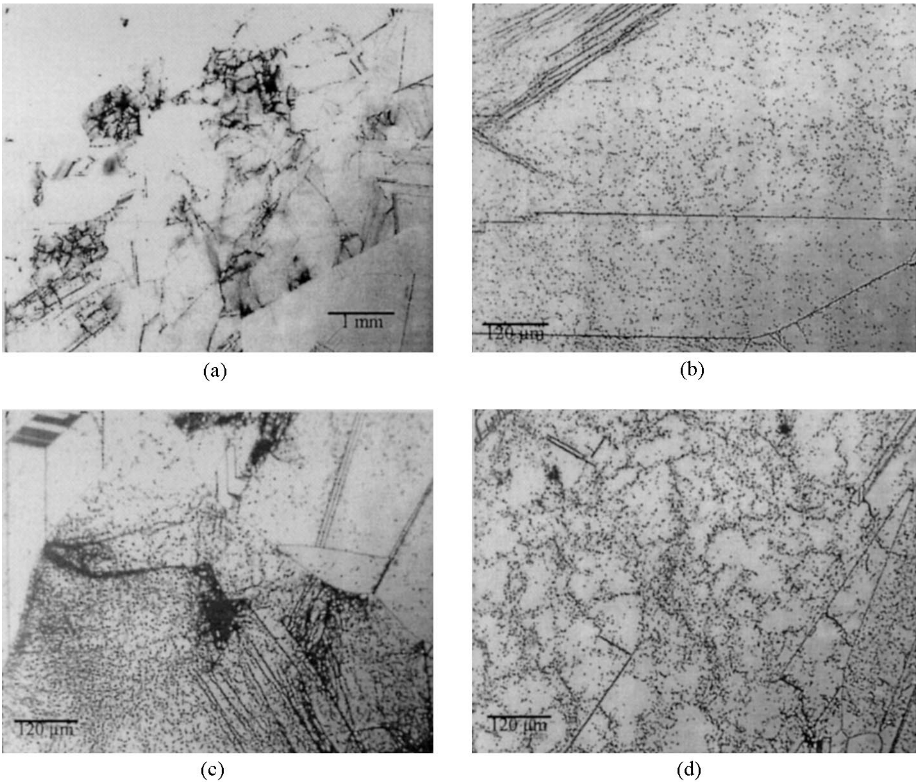

Fig. 3. Etched pits on EPM-Madylam-EMC ingots. Areas of large and low dislocation density are adjacent as shown in (a). (b) Area of dislocations are isolated in the grains. (c) The movement of dislocations is hampered by the presence of grain boundaries. (d) Arrangement of dislocations in cell-like shape.

growth process, the strain is tensile at high temperatures and compressive at lower temperatures [6]. This thermal cycle could be responsible for such an arrangement.

3.3. Impurity contents

The analysis of metallic impurities is performed by atomic absorption spectroscopy. A significant concentration of iron ($0.5–1 \times 10^{16}$ cm^{-3}) and aluminum ($1–4 \times 10^{17}$ cm^{-3}) are found in the EMC materials. By contrast, the Polix material contains a lower level of metallic concentration ($< 5 \times 10^{15}$ cm^{-3}).

Fourier transform infrared spectroscopy (FTIR) has been carried out to measure substitutional carbon and interstitial oxygen concentration in the different multicrystalline silicon substrates. As shown in Table 1, the EMC materials contain a very low oxygen content compared to the feedstock and Polix ingots (about 5×10^{17} cm^{-3}). The oxygen concentration in EMC materials is lower than the detection limit of the system which amounts to 2×10^{16} cm^{-3}. The oxygen is evaporated to the gaseous

Table 1
FTIR measurements of the interstitial oxygen and substitutional carbon concentration in the different multicrystalline materials

Material	EPM-Madylam EMC	SITIX EMC	Polix
Oxygen concent. (cm^{-3})	0.4×10^{17}	$< 0.2\times1017$	6.7×10^{17}
Carbon concent. (cm^{-3})	3.5×10^{17}	3.4×10^{17}	5×10^{17}

atmosphere in the form of gaseous SiO. The carbon concentration does not change during the casting process. No decarburization is observed in the cold crucible melting.

4. Electrical investigations

4.1. LBIC measurements

The light-beam-induced current (LBIC) technique is applied to study the variation in the short circuit current due to the presence of recombining defects inside the poly-Si grains and at grain boundaries. The light beam source is a GaAs laser diode (780 nm) used under a low-frequency mode. Semi-transparent Schottky diodes are realized by evaporating a 20 nm thick chromium layer on the substrate. A silver dot is also deposited on a part of the chromium layer to minimize the series resistance. To avoid any heating of the samples after the realization of the Schottky contact, the ohmic contact is obtained by applying a thin layer of the eutectic Ga–In alloy. The spatial distribution of $i(x, y)$ is detected by a lock-in amplifier through a voltage–current converter and the incident photon flux $I_{ph}(\lambda)$ is carried out using a calibrated photodiode. Thus, the intergranular minority carrier diffusion length (L_D) is obtained by the laser diode scanning away from the junction as proposed by Ioannou and Davidson [7]. The analysis of the electrical activity of as-grown materials has been carried out on different samples sliced in the centermost region of the ingot. The results are reported in Table 2. For the EMC EPM-Madylam material, the mean values of L_D observed are the lowest and for the polix material, the mean value of L_D is conformably close to the literature values for this material.

The minority carrier diffusion lengths of a small point area across the full length of the 120 mm wafer surface are measured. Fig. 4 shows that minority carrier diffusion length is small at the edge of the wafer but it rises gradually from the outer side to the inside. L_D becomes as large as 45 μm at 15 mm inside the wafer. The diffusion lengths beyond 15 mm inside almost represent a uniformity. The distribution of the minority carrier diffusion length across the ingot cross-section is in accordance with the crystal growth pattern shown in Fig. 2. Indeed, it indicates that the small grained chilled layer and poor crystallographic structure near the lateral surface lead to the degradation of electrical properties.

Table 2
Average values of L_D for the different materials

Material	EPM-Madylam EMC	SITIX	Polix EMC
L_D av. (μm)	45	75	90

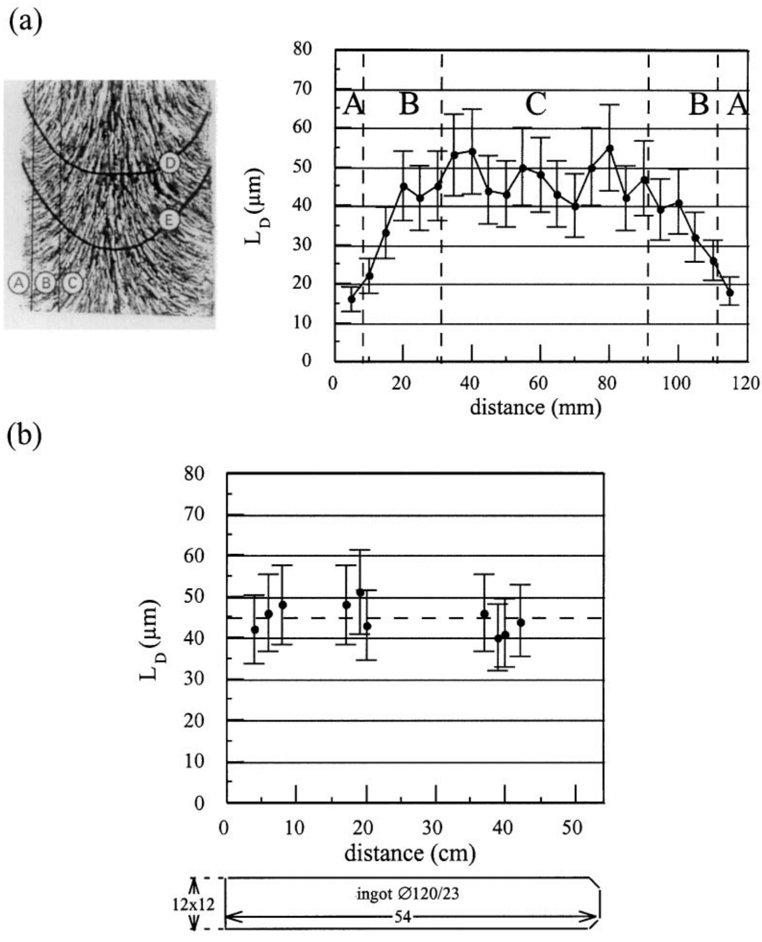

Fig. 4. Measurements of minority carrier diffusion length: (a) on the wafer cross section. The results are in accordance with the crystal growth pattern shown in the inset; (b) along the length of ingot.

In Fig. 4b, the minority carrier diffusion lengths of the ingot shown as a function of a 50 cm length of the ingot did not show a large deviation of L_D throughout the whole length of the ingot. This means that the ingot retains a uniform crystalline property in the pulling direction.

For a more detailed electrical analysis, the LBIC technique is applied to study the variation in the short circuit current due to the presence of recombining defects in a non-processing material. Typical LBIC contrast maps are shown in Fig. 5. The dark areas correspond to regions presenting a smaller local current. In the case of Polix material, a good homogeneity of the induced current is observed inside the grain, while heterogeneity is visible for EMC materials (more pronounced for EPM-Madylam material). Furthermore, although all grain boundaries do not react in the same way due to their orientation and initial impurity density, we observe that the recombination of most grain boundaries for the Polix materials is stronger than that for EMC materials.

4.2. Photovoltaic properties

Solar cells are fabricated on p-type Polix and EMC (SITIX and EPM-Madylam) substrates with standard cell processing reported here: wafers are etched to remove

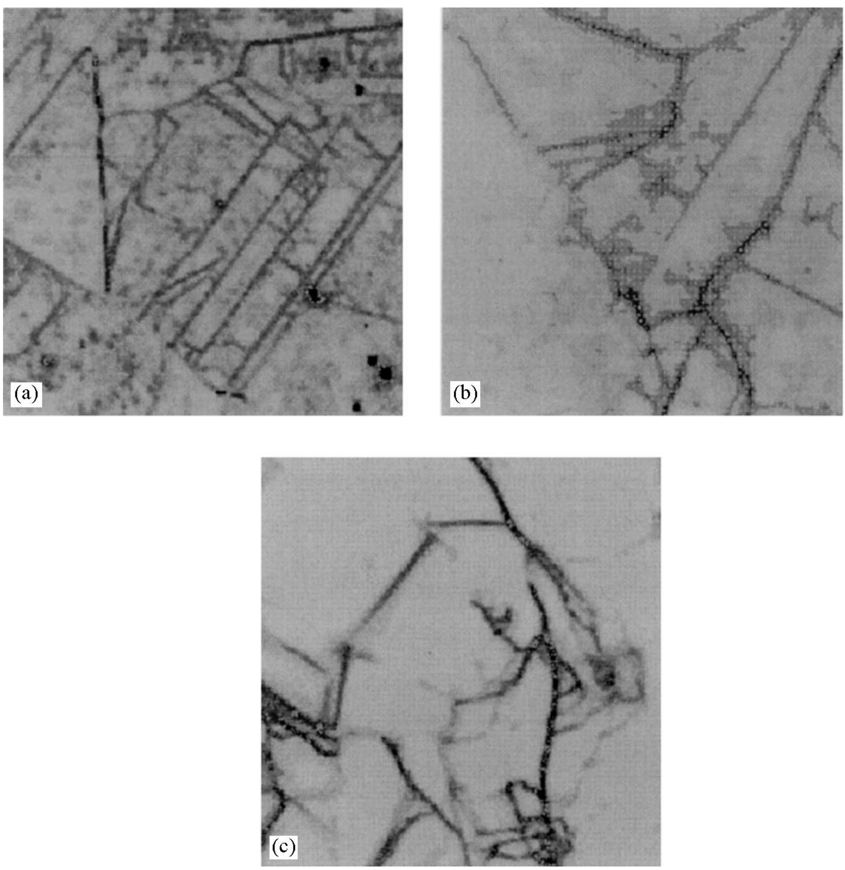

Fig. 5. Typical $2 \times 2\ \mathrm{mm}^2$ LBIC contrast map on the (a) EPM-Madylam-EMC, (b) SITIX-EMC and (c) Polix multicrystalline silicon.

Table 3
Electrical parameters of $100 \times 100\ mm^2$ multicrystalline silicon solar cells using SITIX and EPM-Madylam EMC and Polix substrates under 1.5 at 25°C

Material	EPM-Madylam EMC	SITIX EMC	Polix
Thickness (μm)	205	305	205
Resistivity (Ω cm)	0.75	0.65–0.70	0.48
Surface (cm^2)	96	100	100
V_{OC} (mV)	568	581	602
J_{cc} ($mA\ cm^{-2}$)	23.64	26.56	29.32
FF (%)	70.3	75.9	77.2
η (%)	8.75	11.7	13.5

Table 4
Electrical parameters of $60 \times 60\ mm^2$ multicrystalline silicon solar cells using SITIX and EPM-Madylam EMC and Polix substrates under 1.5 at 25°C

Material	EPM-Madylam EMC	SITIX EMC
Thickness (μm)	205	305
Resistivity (Ω cm)	0.75	0.65–0.70
Surface (cm^2)	36	36
V_{OC} (mV)	569	582
J_{cc} ($mA\ cm^{-2}$)	23.17	27.28
FF (%)	74.6	78.2
η (%)	9.84	12.43

the observed damages and the peripheral region. Their electrical parameters are listed in Table 3. Conversion efficiencies as high as 14% have been obtained in Polix cast silicon, 12% for SITIX and 9% for EPM-Madylam-EMC materials. A significant increase in solar cells performance for EMC-materials is reached when the peripheral region is removed, as indicated in Table 4. Indeed, the baneful influence of the peripheral region is increased for the EMC materials due to the crystallization process: (i) nucleation from the lateral surface of the ingot, (ii) grain orientation according to the solidification interface and (iii) increase of the grain size.

To measure the spectral response, $2 \times 2\ cm^2$ cells are realized in the center of the wafers where the grain size is more important and homogeneous. The external quantum efficiencies of the cells of EMC and Polix are displayed in Fig. 6. The spectral response of the Polix material is significantly higher than that of the EMC cell especially in the long wavelength region. This feature confirms the smaller minority diffusion length for the EMC cells.

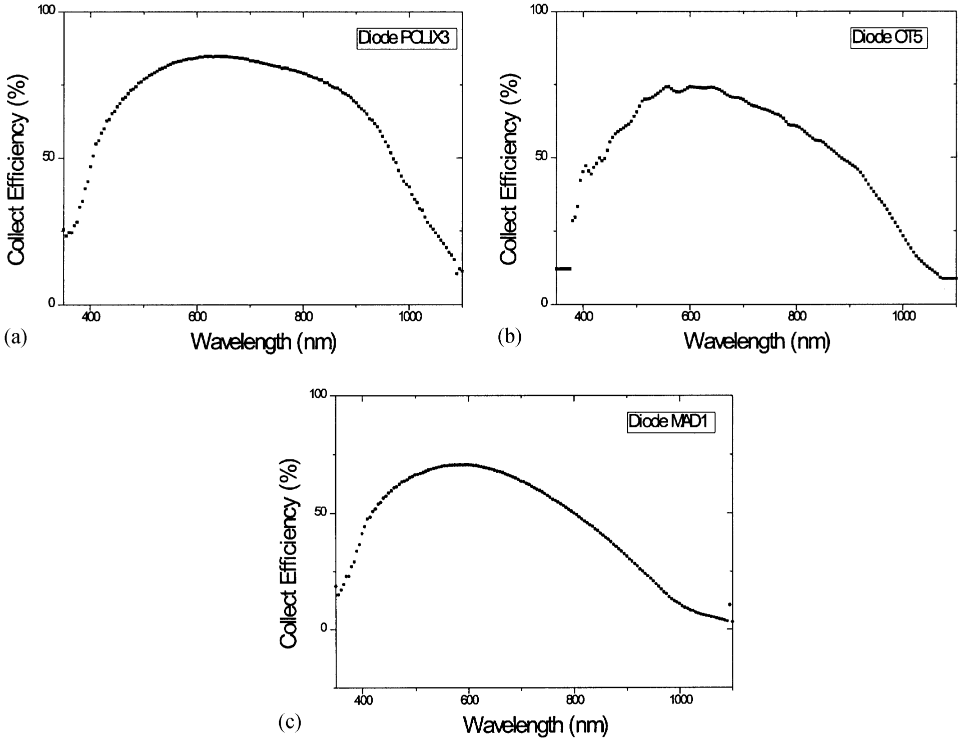

Fig. 6. External quantum efficiency of the $4 \times 4\ cm^2$ solar cells fabricated from (a) Polix, (b) SITIX-EMC and (c) EPM-Madylam-EMC substrates.

5. Effect of thermal treatments

The evolution of minority carrier diffusion length (L_D) during the thermal treatments of solar cell fabrication stages is studied. This thermal cycle is performed on different polycrystalline silicon samples. The sequence of the thermal treatments is reported in Table 5. The dislocation density is estimated to be in the range of $2–4 \times 10^5\ cm^{-2}$ for SITIX EMC and EPM-Madylam EMC samples and in the range of $7–8 \times 10^4\ cm^{-2}$ for Polix samples. The LBIC technique is performed on the different non-processing materials. $1 \times 1\ cm^2$ samples are used and a slight etching is applied to remove the slice damage and surface contamination. LBIC scans are performed on the same sample area before and after annealing. This is a direct evidence of the electrical property variation of samples. The initial schottky structure is removed chemically and remade afterwards to permit LBIC characterization. The values of L_D are obtained by taking an average of 16 measurements. The error on this determination is estimated to be nearly 10%.

Table 6 reports the change of L_D with respect to the initial value L_{D0}, given by $\Delta L_D/L_{D0} = (L_{D0} - L_D)/L_{D0}$ as a function of the thermal treatments. From these

Table 5
Thermal treatment sequences applied to the different multicrystalline samples. For the B series, an annealing treatment under N_2 at 850°C for 30 min is performed on the different materials

Series No.	A	B	C	D	E	F	G	H	I
Diffusion (85°C, 30 min)	×	× ×		×		×			×
Oxidation (850°C, 30 min)			×	×		×			×
Contact firing (850°C, 30 min)					×	×	×		×
Contact annealing (850°C, 30 min)							×	×	×

Table 6
Relative variation of L_D for various thermal treatments (see Table 5) applied to the different multicrystalline samples

Series No.	A	B	C	D	E	F	G	H	I
$\Delta L_D/L_{D0}$ (%) EPM-Madylam EMC	− 2	**− 15**	**− 15**	− 8	0	− 8	**− 13**	**− 11**	− 2
$\Delta L_D/L_{D0}$ (%) SITIX EMC	**− 16**	**− 19**	**− 16**	**− 22**	− 2	**− 18**	**− 14**	**− 14**	**− 10**
$\Delta L_D/L_{D0}$ (%) Polix	**+ 17**	− 9	− 7	**+ 10**	+ 2	**+ 10**	− 2	− 7	**+ 11**

values, some interesting points can be reported:

1. The diffusion treatment (850°C for 30 min under $POCl_3$) has a different effect according to the processed materials: L_D decreases ($\Delta L_D/L_{D0} = -16\%$) for the SITIX samples, as already reported [8], and L_D increases ($\Delta L_D/L_{D0} = +17\%$) for the Polix samples. This treatment has no effect on the EPM-Madylam EMC samples. To prove that such a phenomenon is related to phosphorus diffusion gettering, an annealing treatment under N_2 at 850°C for 30 min is performed on different materials. The results indicate that L_D decreases for all the samples: $\Delta L_D/L_{D0} = -15\%$ for EPM-Madylam EMC, $\Delta L_D/L_{D0} = -19\%$ for SITIX EMC material and $\Delta L_D/L_D = -9\%$ for the Polix material.
2. The contact firing treatment (700°C, 2 min under N_2) does not significantly modify L_D for the different samples.
3. The contact annealing treatment (450°C, 15 min, under N_2) decreases L_D for both EMC samples ($\Delta L_D/L_D = -11\%$ for EPM Madylam and $\Delta L_D/L_D = -14\%$ for SITIX samples), and has no effect on the Polix samples. Moreover, when a thermal sequence like phosphorus diffusion, oxidation and firing treatments is applied prior to this treatment, L_D increases slightly for EMC samples and has no effect as previously observed on Polix material.

In Fig. 7, the relative variation of L_D is represented as a function of the successive thermal treatment applied in the solar cell process. It is interesting to mention that the complete thermal cycle of solar cells fabrication steps has a slight effect on the minority carrier diffusion length ($\Delta L_D/L_D = -2\%$ for EPM Madylam,

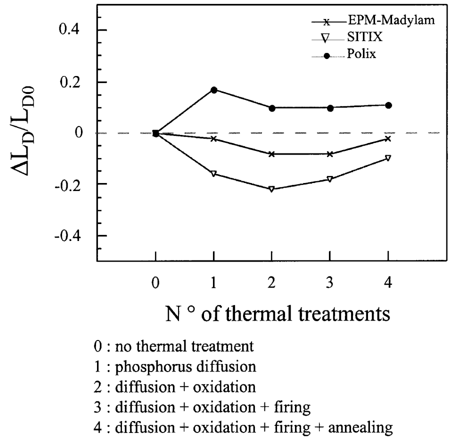

Fig. 7. Relative variation of L_D represented as a function of the successive thermal treatments applied in the solar cell process.

$\Delta L_D/L_D = -10\%$ for SITIX and $\Delta L_D/L_D = +11\%$ for Polix samples). However, as reported previously, the same thermal process induces different electrical behaviors on the different materials.

6. Discussion

The geometry of the crystallization front determines strongly the intergranular structural defect and the grain boundary density of multicrystalline materials [9]. The Polix material is characterized by large grains which nucleate at the ingot bottom and are propagated stably through the growing ingot. The crystallization is performed by extraction of heat through the bottom of the quartz crucible. On the other hand, EMC material is characterized by smaller grains which nucleate from the lateral surface of the ingot. EMC ingots show an heterogeneous grain structure due to a strongly concave solidification interface and suffer from large non-uniformly distributed strains. The differences in electrical properties between the casting processes are linked to these structural imperfections.

The Polix material shows a good homogeneity of intragranular electrical properties as shown in the LBIC contrast maps. However, in this material, the grain boundaries and the bundles of dislocations have a strong recombination. In the materials with a low level of metallic impurity, the electrical activity of extended defects would be, in fact, almost controlled by the oxygen to carbon ([Oi]/[Cs]) ratio. Some authors [10,11] have demonstrated that, in the presence of oxygen, the electrical activity of dislocations and grain boundaries is increased. The carbon content is simply associated with the increase in the dislocation density. In the Polix material, the extended defects have a slight influence on the photovoltaic performance as a consequence of the large grains and the low density of dislocation bundles.

The EMC materials, particularly the EMC EPM-Madylam materials, exhibit a more pronounced recombination activity in the grain. This electrical activity is associated with extended defects inside the grain. Regions of high density of dislocations can be found in the EMC materials. These regions induce a strong recombination of free carriers as presented in the LBIC maps. However, the recombination strength of these extended defects does not seem to be as important as in Polix materials. This result is quite surprising. The strong metallic impurity concentration of iron should provide a strong recombination at extended defects. TEM investigations (not shown) of as-grown EMC material do not reveal any precipitates located either in grain boundaries or near the regions of high density of dislocations. However, since the TEM investigations only reveal precipitates or agglomerates larger than a few nanometers, smaller precipitates or agglomerates remain undetermined. So, the formation of small clusters or metallic-dopant pairs could explain the smaller electrical activity of our samples. As previously reported in literature, FeB pairs could be present and are slightly recombining [12]. The hypothesis of the metallic impurity being in an electrical inactive form is consistent with our results. Moreover, as observed during subsequent thermal treatment (see Table 6), the pairs or the small nuclei with iron would dissociate. The intragranular electrical activity is also increased. Otherwise, we have found that grain boundaries are mostly inclined to recombine although it is reported that the height of the grain boundary barrier in a carbon-rich sample is large [9]. The analysis of the dependence of the minority carrier diffusion length on the microstructure show the great variety of GB types and the associated LBIC contrast. However, EMC materials are characterized by a large density of twin boundaries. It indicates that the electrical activity of the EMC multicrystalline silicon is not dominated by grain boundary recombination. So, the origin of extended defects seems to be of intrinsic nature and the existence of electrical activity, as shown in the LBIC contrast maps, seems to be due to dissolved impurities and small impurity clusters segregated in grain boundaries and extended defects.

7. Summary and conclusion

It appears that the main limiting factor for Polix casting process is close to the content of oxygen and metallic impurities due to contamination from the crucible and the feedstock. For the EMC processes and particularly for EPM-Madylam, the main limiting factor is the crystallographic defects in the shape of small grains and bundles of dislocations decorated by metallic impurities. However, these crystallographic defects do not seem to involve a strong recombination in the entire cell. Thereby, solar cell performances are suitable to the photovoltaic material production. On the other hand, the features of electromagnetic casting reducing cold crucible wear out and permitting a continuous melting and casting of the silicon ingot offer an advantageous economical aspect in comparison with the conventional casting process.

Acknowledgements

Dr. K. Kaneko from Sumitomo Sitix Corp. and Dr. G. Dour from EPM-Madylam are greatly acknowledged for supplying the electromagnetic cold crucible casted multicrystalline silicon material.

References

[1] K. Kaneko, R. Kawamuro, H. Mizumoto, T. Misawa, Proc. 11th Eur. Communities Solar Energy Conf., Montreux, 1992, p. 1070.
[2] S. Martinuzzi, Rev. Phys Appl. 22 (7) (1987) 637.
[3] S. Pizzini, A. Sandrinelli, M. Beghi, D. Narducci, P.L. Fabbri, Rev. Phys. Appl. 22 (1987) 631.
[4] J.R. Davis, A. Rohatgi, R.H. Hopkins, P.D. Blais, P. Rai-Choudhuri, J.R. MacCormick, H.C. Mollenkopf, IEEE Trans. Electron Devices ED-27 (4) (1980) 677.
[5] D. Walton, B. Chalmers, Met. Trans. 215 (1959) 447.
[6] G. Dour, Ph.D Thesis, ENPG, Grenoble, France 1995.
[7] D.E. Ioannou, S.M. Davidson, J. Phys. D 65 (1987) 814.
[8] E. Ehret, V. Allais, J.-P. Vallard, A. Laugier, Sci. Eng. B 34 (1995) 210.
[9] W. Koch, W. Krumbe, I.A. Schwirtlich, Proc. 11th Eur. Communities Solar Energy Conf., Montreux, 1992, p. 518.
[10] S. Pizzini, F. Borsani, M. Acciarri, Mater. Sci. Eng. B 4 (1989) 353.
[11] H. Amzil, L. Ammor, E. Psaila, M. Zehaf, G. Mathian, S. Martinuzzi, J.P. Crest, J. Oualid, B. Pichaud, F. Minari, J. Phys. C 4, T40 (1983) 415.
[12] A. Poggi, E. Susi, M.A. Butturi, M.C. Carotta, J. Electrochem. Soc. 135 (1) (1988) 155.